Selective oxidation of cyclohexane: Ce promotion of nanostructured manganese tungstate

Inês Graça[1], Saeed Al-Shihri[2], David Chadwick[1]*

[1] Department of Chemical Engineering, Imperial College London, South Kensington, London SW7 2AZ, UK

[2] King Abdulaziz City for Science & Technology, P.O. Box 6086, Riyadh 11442, Saudi Arabia

*Corresponding author: d.chadwick@imperial.ac.uk

Abstract

Cyclohexane selective oxidation over nanostructured $MnWO_4$ promoted with increasing amounts of Ce (1-5 wt%) has been investigated at mild conditions using molecular oxygen as oxidant. $MnWO_4$ nanorods were found to be an active catalyst for cyclohexane selective oxidation with selectivity to KA oil (cyclohexanol+cyclohexanone) of approximately 85%. The catalytic performance was improved by impregnation with 1wt% Ce while the textural properties and crystallinity were preserved and Ce was well-dispersed on the surface. XPS analysis of 1%Ce-$MnWO_4$ showed Ce to be present mainly as Ce^{3+}, which is known to promote oxygen adsorption, activation, and mobility. At higher Ce content, the proportion of Ce^{4+} increased to be the main Ce species and large, heterogeneously-dispersed Ce oxide particles are formed on the catalyst surface. The lower Ce^{3+} content reduces the promoting effect while the large Ce oxide particles block access to the active sites on the surface of the $MnWO_4$ nanorod. $MnWO_4$ and 1%Ce-$MnWO_4$ nanorods were shown to retain their selective oxidation performance in consecutive reaction runs. Surprisingly, physical mixtures of nanostructured $MnWO_4$ and a CeO_2 nanopowder showed enhanced selective oxidation activity compared to $MnWO_4$ alone reaching a plateau at 25-50wt% CeO_2, whereas CeO_2 nanopowder itself was found to to be inactive at the reaction conditions. Ce promoted $MnWO_4$ shows promise as a catalyst for selective oxidation of cyclohexane and performs at least as well as the most active non-metallic heterogeneous catalysts reported in the literature.

Keywords: Cyclohexane; selective oxidation; $MnWO_4$; cerium; KA oil.

1. Introduction

The selective oxidation of alkanes remains one of the challenging areas in modern catalysis owing to the relative stability of the CH bond in saturated hydrocarbons, the reactivity of the desired intermediate oxygenate products, and the need to avoid deep or over-oxidation. Despite the difficulty, the challenge is of keen interest due to the great economic benefit of obtaining the intermediate oxygenates for the production of chemicals and polymers from a less expensive and readily available, although very stable, hydrocarbon feedstock [1-3]. Among the several important selective oxidation reactions, one of particular industrial relevance is the selective oxidation of cyclohexane for the production of cyclohexanol and cyclohexanone, also known as KA oil. These are intermediates in the synthesis of adipic acid and caprolactam, which are important precursors for the manufacture of nylon-6,6 and nylon-6 polymers respectively [4-5].

The current commercial cyclohexane selective oxidation process operates in the liquid phase at mild temperature, 150-160ºC, and 10 to 20 bar of oxygen or air pressure, using cobalt or manganese salts as homogeneous catalysts [4-8]. Due to the very high reactivity of the KA oil, cyclohexane conversion is usually kept at a low level (4-6%) to prevent further oxidation of the desired products into acids and esters. At these levels of conversion a high selectivity (70-85%) to cyclohexanol and cyclohexanone can be maintained, thereby reducing product separation and process energy costs. Besides selectivity, another drawback of the process is the highly polluting homogeneous catalyst and its costly separation from the products. Therefore, in view of the increasing demand for these oxidation products and the relatively high environmental impact of this process, continuing attempts have been made to replace the traditional homogeneous catalysts by efficient and more environmentally benign, heterogeneous catalysts.

Heterogeneous catalysts have been studied widely for the selective oxidation of cyclohexane [7-14]. Many have been based on supported transition metals and oxides, such as Ti, V, Cr, Co, Mn, Fe, Mo and Au, supported on silica-based mesoporous material (MCM-41, MCM-48, SBA-15), titanium silicate-1 (TS-1), zeolites (Y, BEA, MOR, MWW, ZSM-5), AlPO molecular sieves and metal oxides (TiO_2, Al_2O_3, SiO_2).

Reasonable cyclohexane conversions (up to about 20%) and selectivities to KA oil (80-90%) can be obtained with these catalysts, but in general they are not very stable due to a high degree of metal leaching [7,9,13,14]. Comparable levels of performance have been achieved with various nanostructured transition metal oxides (7-16% conversion and selectivities >75%), notably Co_3O_4 and mixed Fe-Co oxide nanocrystals [7,15,16]. In addition, the reusability of these materials seems to be superior, as they are reported to maintain their efficiency for 5-6 reaction runs. Some of these catalysts have also been tested using different oxidants, such as hydrogen peroxide (H_2O_2), tert-butyl hydroperoxide (TBHP) and molecular oxygen. Although hydrogen peroxide and TBHP give higher process efficiencies, molecular oxygen (or air) is more desirable because it is relatively cheap, clean, and easy to separate from the catalyst and products, and it is reported to increase the stability of the catalytic species reducing the potential for over-oxidation [9]. A challenge has been to find active, non-noble-metal heterogeneous catalysts for direct selective oxidation using molecular oxygen (or air) as oxidant. In some cases, oxygen has been combined with small amounts of a radical initiator (H_2O_2 or TBHP for instance), to accelerate the initiation step of the oxidation process.

Catalysts based on Mn are attractive oxidation catalysts owing to their facile redox behaviour. For example, Modén et al. [17] showed that MnAlPO was more active than CoAlPO for cyclohexane oxidation with oxygen, and that the reaction rate was dependent on the number of Mn_{redox} sites able to interchange between Mn^{2+} and Mn^{3+}. A study of cyclohexane oxidation by air over unsupported Mn oxides showed the highest cyclohexane conversion was achieved for calcination at 400ºC, which was attributed to the higher surface Mn^{4+} concentration promoting oxygen mobility and increased oxygen adsorption capacity [18]. The use of Mn containing mixed-metal oxides in oxidation reactions has been studied frequently in the literature [19-23]. Mixed metals of variable valency increases oxygen vacancies and enhances oxygen ion mobility. Of particular relevance to the present study are the use of nanostructured $MnWO_4$ in the oxidative dehydrogenation of propane to propene [20], and of $MnCeO_x$ solid solutions for cyclohexane selective oxidation [21,22]. $MnWO_4$ nanorods prepared by hydrothermal synthesis were found to present higher selectivity to propene than bulk Mn oxide, which was attributed to its unique surface structure containing defect-rich MnO_x zigzag chains geometrically isolated by W_2O_8 units.

$MnCeO_x$ solid solutions have shown remarkable results for cyclohexane selective oxidation to KA oil in the liquid at mild conditions [21], and in continuous gas phase reaction at 180°C [22]. Indeed, CeO_2 has been applied extensively in the formulation of catalysts for various oxidation reactions including of carbon monoxide [23,24], alcohols [25,26] and hydrocarbons [21,22,27-30], due to the effectiveness of the Ce^{3+}/Ce^{4+} redox pair in creating oxygen vacancies thereby increasing the oxygen ion mobility and oxygen storage capacity, which can be enhanced by doping transition metals into the ceria cubic fluorite lattice. Based on this literature it seems probable, therefore, that nanostructured $MnWO_4$ [20] might be a promising catalyst for cyclohexane selective oxidation although this has not been investigated to date. Furthermore, due to the wide-spread use and importance of ceria in oxidation reactions, the promotion of $MnWO_4$ by Ce would appear to be a fruitful approach, although again it has not been investigated previously for cyclohexane selective oxidation.

In this work the performance of nanostructured $MnWO_4$ and Ce promoted $MnWO_4$ catalysts in the solventless selective oxidation of cyclohexane has been investigated in the liquid phase at mild conditions using molecular oxygen as oxidant. As noted above, these materials have not been studied previously for the selective oxidation of cyclohexane. We show that $MnWO_4$ nanorods are indeed active, selective catalysts for cyclohexane selective oxidation maintaining good stability in consecutive runs. The impact of Ce on catalytic performance has been investigated by two approaches. In the first approach, Ce was added to the $MnWO_4$ nanostructure by incipient wetness impregnation (1-5 wt%). In the second approach, the activity of mechanical mixtures of the $MnWO_4$ catalyst and a CeO_2 nanopowder (1-50 wt%) has been studied. It is shown that either approach leads to a significant promotion of catalytic activity without loss of selectivity, although CeO_2 itself is not active for cyclohexane oxidation at the reaction conditions used. The influence of reaction time on the conversion to KA oil and selectivity shows the presence of an initiation period and the role of cyclohexyl-hydroperoxide in the oxidation process in agreement with studies of other Mn-based oxidation catalysts.

2. Experimental

2.1 Catalyst preparation

Nanostructured $MnWO_4$ samples were prepared according to the hydrothermal method described in the literature [19,20,31]. Optimum temperature and pH conditions were selected from the literature in order to obtain highly crystalline anisotropic nanorods with the best surface properties for oxidation reactions. For the synthesis, 20 mL of a 0.2M aqueous solution of $Mn(NO_3)_2 \cdot 4H_2O$ (Alfa Aesar, 98%) were firstly added drop-wise to 20 mL of a 0.2M aqueous solution of $Na_2WO_4 \cdot 2H_2O$ (Sigma, ≥99%), while vigorously stirring at room temperature. Afterwards, a 0.1M NaOH aqueous solution was added under stirring until pH 10 was reached. The suspension obtained was transferred into a 50 mL PTFE-lined stainless steel autoclave, which was kept at 180ºC overnight in an oven. After naturally cooling down to room temperature, the solid was filtered, washed with deionised water and dried overnight in an oven at 100ºC. Finally, the catalyst was calcined under nitrogen at 400ºC for 2h.

1-5 wt% of cerium was introduced on the nanostructured $MnWO_4$ by incipient wetness impregnation using $Ce(NO_3)_3 \cdot 6H_2O$ (Aldrich, 99%) as precursor salt. An aqueous solution of the Ce salt with a very small amount of water was added drop-wise to the $MnWO_4$, while stirring. After impregnation, the samples were dried overnight in an oven at 100ºC and calcined under air at 500ºC for 3h to obtain cerium oxide. Mechanical mixtures of 1-50 wt% CeO_2 and $MnWO_4$ were also prepared by mixing a commercial CeO_2 nanopowder (Aldrich, <25 nm particle size) with the as-synthesised $MnWO_4$ nanostructured solid.

2.2 Catalyst characterisation

W and Mn contents on the parent $MnWO_4$ nanorods were determined by inductively coupled plasma optical emission spectroscopy (ICP-OES) using a Varian Vista MPX ICP-OES system.

XRD patterns were obtained with a PANalytical X'Pert Pro diffractometer using Cu Kα radiation operating at 40 kV and 40 mA. The scanning range was set from 10° to 60° (2θ), with a step size of 0.033º and step time of 20s.

BET specific surface area was determined by N_2 adsorption at -196ºC on a Micrometrics TriStar apparatus. Before adsorption samples were degassed under nitrogen flow at 350ºC overnight.

Transmission electron microscopy with energy-dispersive X-ray spectroscopy (TEM-EDS) was performed by using a JEOL2010 Transmission Electron Microscope operating at 200 kV coupled with a X-MaxN 80T Silicon Drift Detector from Oxford Instruments. The samples were prepared by dispersing a small amount of solid in ethanol and adding a drop to a copper grid coated with holey carbon film.

X-ray photoelectron spectroscopy (XPS) were recorded on a Thermo K-Alpha Spectrometer equipped with Al Kα source gun using an X-ray spot size of 400 μm and pass energy of 20 eV. Samples were mounted on double-sided adhesive tape and the spectra were collected with 0.1 eV increments. The binding energies (BE) were referenced to the C 1s peak of adventitious carbon at 284.8 eV. Data analysis and peak fitting were performed using Avantage software from Thermo Scientific.

Spent catalysts were analysed for carbonaceous deposits using thermogravimetric analysis (TGA) in a TA Instruments TGA Q500. Samples were heated up from room temperature to 800°C at 10°C/min under air flow (60 mL/min). The nature of the carbonaceous deposits was investigated by infrared spectroscopy using a PerkinElmer Spectrum 100 FTIR spectrometer, equipped with a Specac ATR (attenuated total reflection) unit.

2.3 Catalytic activity measurement

Cyclohexane oxidation was performed in a 25 mL Büchi AG steel autoclave at 140 or 150°C using a PTFE liner under initial cold pressure of 10 bar of pure oxygen. Typically, 4 g of cyclohexane (Riedel-de Haën, ≥99.5%) and 0.095 g of catalyst were introduced into the reactor. The reactor was sealed, purged with oxygen 3 times and the initial working pressure set. A silicone oil bath was used to heat up the reactor. The reactor was introduced to the bath after the desired temperature was reached to minimise effect of the heat up time which was about 10 min. The reaction was carried out for 1-8h under continuous stirring at 600 rpm to have a well-mixed condition and avoid diffusional limitations. Conversion was shown to be independent of stirring speed 600 – 1000 rpm. After reaction, the reactor was removed from the oil bath and

cooled down using an ice bath, the oxygen was released and the liquid product-catalyst suspension collected. The catalyst was separated from the mixtures by centrifugation at 5000 rpm for 5 min. Liquid samples were analysed by gas chromatography using a Shimadzu GC-2014 gas chromatograph with an Agilent CP-Wax 52 CB UltiMetal column and FID detector. 1,2-dichlorobenzene (Sigma-Aldrich, 99%) was added as a standard. Each sample was analysed with and without addition of triphenylphosphine (Sigma-Aldrich, ≥95%), which converts the cyclohexyl-hydroperoxide still remaining in the liquid product into the corresponding alcohols [32]. The difference between the cyclohexanol amount before and after triphenylphosphine addition was used to obtain the cyclohexyl-hydroperoxide content. Cyclohexane conversion to KA oil was calculated from the sum of cyclohexanol, cyclohexanone and cyclohexyl-hydroperoxides molar yields. Several runs were repeated to establish the reproducibility of the conversion and selectivity. These were selected to be representative of temperature, time and catalytic material. Values of standard deviation in the conversion to KA oil and selectivity are given in the appropriate figure caption. It is assumed that similar standard deviations apply to non-repeated data points. Carbon oxides were determined using a Shimadzu GC-14B with a Carboxene 1000 60-80 mesh packed column and TCD detector.

3. Results and Discussion

3.1 Catalyst characterisation

3.1.1 Nanostructured $MnWO_4$

The phase purity of the as-synthesised $MnWO_4$ material was verified by XRD (Fig. 1). A manganese tungstate with a pure monoclinic wolframite-type structure was obtained in good agreement with the literature [20,31,33]. The BET specific surface area of the $MnWO_4$ prepared in this work (Table 1) has a BET specific surface area that is about half the values commonly reported in the literature [19,20]. Despite this difference, the TEM micrographs (Fig. 2a) show that $MnWO_4$ in the shape of nanorods with ~100-250 nm length and ~30-50 nm width was in fact formed by the hydrothermal synthesis [19,31]. The crystallinity of the $MnWO_4$ nanorods was also confirmed by TEM and SAED (Fig. 2a).

XPS of the $MnWO_4$ nanorods is shown in Fig. 3. The Mn 2p XPS shows two main peaks arising from the Mn $2p_{3/2}$ and Mn $2p_{1/2}$ states (Fig. 3a), each showing evidence of two strong component peaks and an associated high binding energy satellite (at 646 eV for Mn $2p_{3/2}$). Mn 2p spectra of Mn compounds do not always show a clear variation with oxidation state [34-36]. However, the main Mn 2p peak at 640.4eV is consistent with Mn being present mainly as Mn^{2+} [18-20,34-39], while the shoulder at higher binding energy probably arises from a mixture of Mn^{3+} and Mn^{4+} [18,34-39]. Deconvolution suggests the proportion of Mn in a higher valency to be about 52%. The W 4f XPS spectrum (Fig. 3b) shows the presence of the doublet W $4f_{7/2}$ and W $4f_{5/2}$ at 35.5 and 37.6 eV in agreement with the binding energies found in the literature for metal tungstates, corresponding to W^{6+} [19,33]. A more detailed analysis reveals a much less intense doublet at approximately 36.2 and 38.1 eV, which indicates the presence of W-OH groups at the surface of the $MnWO_4$ nanorods [19]. The O 1s XPS spectrum (Fig. 3c) presents a main peak at 530.4 eV arising from bulk lattice oxygen (O_α), and smaller peaks at 532.4 and 533.2 eV, which are typically related to surface oxygen, oxygen defects or OH (O_β), and chemisorbed water and/or carbonates respectively [19,22,24,38]. The surface composition based on XPS (63.3 wt% W, 15.8 wt% Mn, 20.9 wt% O, Supporting Information Table S.1) is a reasonable match to the composition determined by elemental analysis: 56.8 wt% W, 16.8 wt% Mn , 26.4 wt% O. Therefore, $MnWO_4$ nanorods similar to those previously described in the literature [19,20,31] were synthesised successfully.

3.1.2 Ce impregnation

As-synthesised $MnWO_4$ nanorods were impregnated with increasing Ce contents (1-5 wt%). A pronounced reduction of the relative intensity of the $MnWO_4$ XRD peaks can be observed after Ce impregnation (Fig. 1). This could be due to a decrease of the $MnWO_4$ nanorods crystallinity, but the Ce contents on the catalysts are not so high to justify a loss of crystallinity of about 24-35% (Table 1). It has been reported in the literature that Ce has a very high absorption coefficient of X-ray radiation, which could explain the significant reduction of the XRD peaks intensity in the presence of this rare earth element [40,41]. No peaks related to the fluorite structure of the CeO_2 (2θ = 28.6, 33.3, 47.5 and 56.5º) can be seen in the XRD of the samples containing Ce. No significant modifications to the shape of the $MnWO_4$ nanorods are visible by

TEM when 1 wt% of Ce is impregnated (Fig. 2b). Analysis by EDS was difficult owing to the low level of Ce. However, the measured value was 1wt%Ce and no local high concentrations of Ce were found. Therefore, XRD and TEM show clearly that for 1wt%Ce, the Ce is well-dispersed on the $MnWO_4$ surface. In sharp contrast, cerium oxide particles of about 10-20 nm were found on the surface of the $MnWO_4$ nanorods containing 5 wt% Ce (Fig. 2c). The cerium oxide particles appear to be agglomerates and poorly crystallised or amorphous (Fig. 2d) consistent with the absence of CeO_2 peaks in XRD. EDS analysis of 3 and 5wt% Ce catalysts at several points (Supporting Information Table S2) confirmed that the Ce oxide particles are heterogeneously distributed over the surface of the $MnWO_4$ at the higher Ce contents. The BET specific surface area is not significantly affected by the addition of Ce, Table 1, with only a slight decrease being observed for the sample containing the highest amount of Ce (5 wt% Ce).

XPS for the Ce impregnated catalysts was performed on selected samples: 1%Ce-$MnWO_4$, which proved to be the most active of the promoted catalysts (see below), and 5%Ce-$MnWO_4$. The surface compositions determined from XPS are given in Supporting Information Table S.1. The Mn peaks are relatively more reduced by Ce impregnation compared to W consistent with the more surface sensitive nature of the Mn 2p peaks. The value for Ce is close to the nominal loading for 1%Ce impregnation indicating Ce is well-dispersed over the surface and might suggest some penetration into the near surface region of the nanorods. For the 5% Ce sample, the Ce from XPS is higher than the nominal loading consistent with the presence of Ce oxide particles over the surface of the $MnWO_4$ nanorods.

In the XPS of the Ce promoted $MnWO_4$ there is no significant change in either the Mn 2p or W4f spectra for low levels of Ce impregnation (Fig. 4a, b), so that the oxidation states of Mn and W appear to remain essentially unchanged by 1%Ce impregnation. For higher Ce loading there is a broadening of the Mn 2p and W 4f spectra and small binding energy shifts, Fig. 4a and b, compared to unpromoted $MnWO_4$ (Fig. 3). This is consistent with the presence of the large Ce oxide particles heterogeneously distributed over the surface causing local variations in the chemical environment. The proportion of Mn as Mn^{3+} and Mn^{4+}, however, does not appear to change significantly at 5wt% Ce impregnation, Fig. 4a. The Ce 3d XPS is complex and composed of two multiplets (v and u) corresponding to the Ce $3d_{5/2}$ and Ce $3d_{3/2}$

core holes and in cerium oxide materials both multiplets have contributions from the Ce^{3+} and Ce^{4+} oxidation states [24,38,42-45]. The Ce 3d XPS of 1%Ce-$MnWO_4$ (Fig. 4d) has the general appearance of Ce^{3+} and there is only a small peak at about 917.0 eV, which is attributable solely to Ce^{4+}. The proportion of Ce^{3+} was estimated to be approximately 70%. Cerium tungstate is a Ce(III) compound and CeO_2-WO_3 solid solutions have Ce and W in the form of Ce^{3+} and W^{6+} respectively [44,45]. The presence of such a high fraction of Ce^{3+} in 1%Ce-$MnWO_4$ may indicate, therefore, that a significant fraction of the Ce is doped into the surface of the $MnWO_4$ nanorods. The XPS of 5%Ce-$MnWO_4$ shows a greatly increased proportion of Ce^{4+} over Ce^{3+}, estimated to be approximately 70% Ce^{4+}. This is consistent with the oxide particles on the surface of the nanorods seen in TEM (Fig 2 c, d) being CeO_2, which also leads to a greater proportion of O_β and chemisorbed species in the XPS O1s spectrum of the 5wt% Ce material, Fig 4c.

3.2 Catalyst performance

The oxidation of cyclohexane was studied in the liquid phase at mild conditions, 140-150ºC and 10 bar O_2. At these conditions a blank reaction showed no detectable conversion of cyclohexane.

3.2.1 Nanostructured $MnWO_4$

The main products of cyclohexane oxidation were observed to be cyclohexane and cyclohexanone (cyclohexyl-hydroperoxide was determined by the addition of triphenylphosphine as described in the experimental section above). A number of minor by-products were detected by GC which were not individually identified but were assumed to be aldehydes, esters and acids as these are commonly observed by-products of this reaction [7,8]. Carbon balances based only on the products cyclohexanol and cyclohexanone were 70-80%. However, this contains a contribution from evaporative loss of cyclohexane during catalyst separation and GC sample preparation despite the application of cooling. Mass loss by evaporation was evaluated by injecting a heavier solvent (decane) to the reaction mixture before opening the reactor and catalyst separation. Carbon balance with solvent injection

increased from 73 to 84%, indicating the by-products contribute approximately 15% of the carbon balance at these conditions. Finally, the gas composition obtained after 4h at 150ºC was also analysed by gas chromatography. Only negligible amounts of CO and CO_2 (around 0.02 mmol in total corresponding to a yield of 0.047%) were detected, showing that the contribution of total oxidation is very low.

Fig. 5 shows the evolution of the conversion to KA oil as a function of the reaction time for the $MnWO_4$ nanorods at 140 and 150ºC. First of all, it is possible to see that the $MnWO_4$ nanorods are active catalysts for the selective oxidation of cyclohexane at both temperatures, yielding a reasonable amount of KA oil in comparison to the literature at the same conditions [8]. The good performance of $MnWO_4$ nanorods for oxidation reactions has been ascribed to the presence of isolated MnO_x chains at the surface of the particles, which are rich in oxygen defects that act as active sites in the activation of hydrocarbons or alcohols and activation of oxygen in a redox process [19,20].

Conversion of cyclohexane to KA oil shows evidence of an initiation time at both 140 and 150ºC and increases sharply thereafter at short reaction times reaching a maximum at about 4h of reaction. The presence of an initiation time is consistent with the known mechanism of reaction which proceeds via cyclohexyl-hydroproxide formation as the initial product [46] as noted below. The decrease of conversion to KA oil observed after 4h could be due to catalyst deactivation and/or further transformation of cyclohexanol and cyclohexanone, since conversion is determined as the sum of the yield of these products. It was noted that the evolution of the normalised total GC area for the by-products with the reaction time followed the yield of KA oil at 150ºC, but increased continuously with time at 140ºC (Supporting Information Fig. S.1 and S.2). Therefore, the decrease of the conversion to KA oil at longer reaction times seems to be related to the production of a higher amount of by-products at 140ºC, whereas at 150ºC deactivation of the catalyst appears to be the main cause of the fall in conversion to KA oil. From TGA measurements on the spent catalysts, the deposition of carbonaceous materials on the catalyst at 150ºC was found to increase with reaction time (1.9-7.2 wt%, Supporting Information Fig. S.5 and Table S.3), which could be the cause of the observed deactivation. The presence of carbon-based compounds on the catalyst after 8h of reaction at 150ºC was confirmed by infrared spectroscopy (Supporting Information Fig. S.7). It was possible to identify

additional peaks on the spent catalyst arising from the presence of C-H, C=O and C-O groups [47]. As the rate of reaction is slower at lower temperature (Table 2), by-products formation at 140ºC might be lighter compounds than at 150ºC and these may desorb more easily from the catalyst.

The selectivity to cyclohexyl-hydroperoxide (Table 3) is observed to be higher at short reaction times consistent with cyclohexyl-hydroperoxide being the initial product in the oxidation sequence. Comparing the cyclohexanol and cyclohexanone selectivities vs. reaction time (Fig. 6), it can be noticed that the selectivity to cyclohexanol is higher than to cyclohexanone at short reaction times at both temperatures. This is in agreement with the expected reaction mechanism and kinetics, as cyclohexyl-hydroperoxide transformation into cyclohexanol is usually faster than into cyclohexanone [46]. With increasing reaction time, cyclohexanol selectivity decreases while cyclohexanone selectivity increases, which is especially evident up to 4h of reaction. This results from the cyclohexanol conversion into cyclohexanone [46] and after 4h of reaction selectivities tend to stabilise at about 50%. Cyclohexanol initial conversion into cyclohexanone is higher at 150ºC as indicated by the lower cyclohexanol selectivities at 150ºC than 140ºC, consistent with the higher initial reaction rate at higher temperature (Table 2).

3.2.2 Ce impregnated catalysts

The catalytic results found for the catalysts impregnated with 1 to 5 wt% Ce at 140 and 150ºC are shown in Fig. 7 in comparison with the parent $MnWO_4$. The data is for a reaction time of 4h. Clearly, the activity of the $MnWO_4$ nanorods is improved through the addition of low amounts of Ce, as conversion increases at both 140 and 150ºC when 1 wt% of Ce is impregnated. This enhancement of the conversion to KA oil by impregnation with Ce arises from the nature of the Ce surface species in the impregnated catalyst. At low Ce loading, Ce is mainly in the form of Ce^{3+} and may be partly doped into the surface layers. This generates surface oxygen vacancies which can be expected to promote the activation of the oxygen molecules [26], thereby enhancing the cyclohexane conversion to KA oil for the 1%Ce-$MnWO_4$ catalyst. The precise location of the Ce promoter induced oxygen vacancies is speculative. They are expected to be mainly in the highly dispersed surface cerium

oxide. However, if Ce^{3+} is also in the surface layers of the $MnWO_4$ then oxygen additional vacancies can be generated in the surface of the $MnWO_4$.

The addition of increasing quantities of Ce by impregnation beyond 1% consistently leads to a decrease of the conversion to KA oil at both temperatures. Conversions to KA oil found for the 3 and 5 wt% Ce impregnated catalysts at both temperatures are even lower than expected considering the amount of $MnWO_4$ present in the final catalysts. Apparently, impregnation of high Ce amounts has a negative impact on the intrinsic activity of the $MnWO_4$ nanorods. This has two potential origins. Firstly, the proportion of Ce^{3+} decreases at high Ce content reducing the capability for oxygen activation. Secondly, the presence of large Ce oxide particles on the surface of the $MnWO_4$ (as observed by TEM, Fig. 2c, d) can partially block access to the active sites on the $MnWO_4$ surface.

The evolution of the conversion to KA oil with reaction time at 140 and 150ºC for the most active impregnated catalyst, 1%Ce-$MnWO_4$, is shown in Fig. 5. First of all, the activity of the catalyst promoted with 1 wt% Ce is always higher than that of the $MnWO_4$ nanorods, whatever the reaction time or temperature. As for the parent $MnWO_4$, an initiation period is observed, which is associated with the initially slow activation of the cyclohexane to produce cyclohexyl-hydroperoxide. Thereafter, evolution of the conversion to KA oil with the reaction time for the 1%Ce-$MnWO_4$ catalyst follows a similar trend as for the parent $MnWO_4$. However, while at 140ºC the maximum conversion to KA oil is observed at 4h of reaction for both catalysts, at higher temperature this occurs around 2h of reaction for the Ce-impregnated material. Indeed, an identical reaction rate after the initiation time was found for both $MnWO_4$ and 1%Ce-$MnWO_4$ catalysts at 140ºC, whereas the catalyst containing 1%Ce presents a much higher reaction rate at 150ºC (Table 2). Conversion to KA oil decays at longer reaction times and appears to be related mainly to catalyst deactivation due to the formation of carbonaceous material at both temperatures (see Supporting Information Figs. S.3 and S.4). However, deactivation is much less pronounced for the Ce-promoted $MnWO_4$, which is in agreement with the lower carbonaceous contents (1.5 - 5.0 wt%) found for the 1%Ce-$MnWO_4$ catalyst (Supporting Information Table S.3), and the well-known ability of ceria to resist coke formation [48].

The variation in selectivities with reaction time is similar for the $MnWO_4$ and 1%Ce-$MnWO_4$ catalysts. Nevertheless, while at 140ºC cyclohexanol and cyclohexanone

selectivities are near-identical for both $MnWO_4$ and 1%Ce-$MnWO_4$ catalysts, selectivities for cyclohexanol are lower for 1%Ce-$MnWO_4$ at 150ºC in agreement with the early reaction rates. Therefore, cyclohexanol and cyclohexanone selectivities appear to depend on the reaction rate over the catalysts. We also note that the cyclohexyl-hydroperoxide selectivity is smaller for the 1%Ce-$MnWO_4$ catalyst than for the $MnWO_4$ nanorods at 150ºC (Table 4), which is consistent with the higher reaction rate over the former at higher temperature. Finally, it was confirmed that, as for $MnWO_4$, CO and CO_2 yields were very low ($CO+CO_2$ = 0.045% yield).

The performance of the present 1%Ce-$MnWO_4$ catalyst for cyclohexane selective oxidation may be usefully compared to the performance of recently reported catalysts based on mesoporous Ce-Mn-oxide solid solutions [21]. Zhang et al. [21] reported cyclohexane conversions of 10.5 and 18.8% after 4h at 120 and 150ºC respectively. Selectivity to KA oil at 120ºC was 84%, but decreased to only 52% at 150ºC where the conversion was highest. As noted above, in the current industrial process conversion is usually kept at a low level of 4 to 6% to maintain high selectivity to KA oil [4-8]. The present 1%Ce-$MnWO_4$ catalyst achieves a KA oil yield of around 7% with selectivity of about 85% (corresponding to a cyclohexane conversion of 8.3%) at 140ºC and 150ºC, Fig. 5. Furthermore, at 150ºC, maximum yield of KA oil is achieved after only 2 h. Indeed conversion to KA oil over 1%Ce-$MnWO_4$ is extremely rapid after the initiation time. The study of Ce-Mn-oxide solid solutions used 50% higher catalyst to cyclohexane ratio [22] than the present study. It would appear, therefore, that the performance of the present 1%Ce-$MnWO_4$ catalyst for cyclohexane selective oxidation is comparable to that reported for Ce-Mn-oxide solid solution catalysts by Zhang et al. [22]. However, the surface area of the most active mesoporous Ce-Mn-oxide solid solution catalyst ($Ce_{0.5}Mn_{0.5}O_x$-500) was reported to be 89 m^2/g [22], compared to only 13 m^2/g for 1%Ce-$MnWO_4$, Table 1. From this comparison we may conclude that 1%Ce-$MnWO_4$ is intrinsically a more active material for selective oxidation of cyclohexane.

3.2.3 CeO_2 + $MnWO_4$ mechanical mixtures

In order to investigate further the interaction between CeO_2 and the $MnWO_4$ nanorods, the selective oxidation of cyclohexane was also carried out over a series of

mechanical mixtures containing increasing amounts of CeO_2 nanopowder (1-50 wt%) at 150ºC for 2h, Fig. 8a. A relatively short reaction time was used to resolve more clearly the effect of the CeO_2 addition, while being significantly longer than the initiation time, Fig. 5. In Fig. 8a, the conversions to KA oil obtained for $MnWO_4$ and 1%Ce-$MnWO_4$ catalysts at the same operating conditions and reaction time are also presented for comparison. It can be observed that the overall conversion to KA oil increases continuously when increasing the proportion of CeO_2 in the mechanical mixtures. The CeO_2 nanopowder alone was found to have no activity. Taking into account that the amount of $MnWO_4$ nanorods in the mixtures is decreasing as CeO_2 is increasing, this demonstrates clearly a synergetic effect between these two materials. The conversion to KA oil increases rapidly with the CeO_2 addition up to 10 wt% of CeO_2 in the mixtures and steadily thereafter up to 20 wt% CeO_2. After 20 wt% CeO_2 the conversion to KA oil reaches a plateau as expected since at even higher levels of CeO_2 the conversion must fall ultimately to zero at 100% CeO_2. Since the initial product of cyclohexane oxidation is cyclohexyl-hydroperoxide and CeO_2 nanopowder is itself inactive, it is tempting to conclude that CeO_2 is not able to initiate the oxidation of cyclohexane at these reaction conditions. Therefore, the beneficial effect of the mixing CeO_2 with the $MnWO_4$ nanorods could result from (i) a possible transfer of Ce to the $MnWO_4$ nanorods due to the contact promoted by the stirring during the reaction, (ii) transfer of Mn to the CeO_2 surface forming Mn-CeO_x solid solution which are known to be active for this reaction [21, 22], (iii) an additional supply of activated oxygen to the $MnWO_4$ nanorods provided by the CeO_2 during the contact, and/or (iv) the additional conversion of cyclohexyl-hydroperoxides formed on the $MnWO_4$ nanorods over the CeO_2 nanopowder. To investigate hypothesis (iv), the CeO_2 was tested alone with the addition of a small amount of initiator (4 mg of tert-butyl hydroperoxide) at 140ºC for 4h. A conversion to KA oil of 10.2% was reached. For comparison, a blank run with only cyclohexane and initiator was also carried out where the yield of KA oil was 8.60%. This means that the CeO_2 nanopowder increases the yield by 18% when the initiator is present showing that the CeO_2 nanopowder is probably capable of converting the cyclohexyl-hydroperoxides once these are formed. Even so, mechanisms (i) to (iii) may be also operative.

Comparing the improvement of the conversion to KA oil at 2 h obtained when adding 1 wt% Ce to the $MnWO_4$ nanorods by impregnation (47% increase) and in the form of

a mechanical mixture with CeO_2 nanopowder (13% increase) (Fig. 8a), it is clear the promotion effect is much greater when Ce is impregnated, consistent with a closer interaction being established by the impregnation method as expected. Another interesting observation with the mechanical mixtures is that an enhancement of the conversion to KA oil with CeO_2 addition is always observed, whereas a decrease of the conversion occurs for the Ce impregnated $MnWO_4$ nanorods with higher amounts of Ce. As there is only transient direct contact between the CeO_2 and the $MnWO_4$ in the mechanical mixtures, we assume that almost all the active sites on the $MnWO_4$ nanorods would always be free to catalyse the reaction. This is consistent with blockage of active sites on the $MnWO_4$ nanorods by CeO_2 particles occurring when Ce is impregnated at higher amounts, as proposed above to account for the decrease in activity observed for these higher Ce loaded catalysts, Fig. 7.

3.2.4 Catalyst stability

Stability of the $MnWO_4$ and 1%Ce-$MnWO_4$ catalysts was investigated by performing three consecutive reaction runs at 150ºC under 10 bar O_2 for 4h, which corresponds to the maximum conversion to KA oil in the first run at this temperature (Fig. 5a). After each run the catalyst was separated from the liquid product by centrifugation, washed three times with acetone and dried at room temperature overnight before being used in the following reaction run. Table 5 and 7 gives the conversions to KA oil, yields and selectivities obtained for each reaction run. It can be seen that both catalysts keep their activity over the three runs. The spent samples after 3 reaction runs were analysed by XRD in order to see if any structural changes take place during the reaction (Fig. 1). It was observed that the structure and crystallinity of both spent catalysts remain unaffected when compared to the fresh samples. A small carbon deposition of about 2% was found by TGA analysis on both samples after the 3 consecutive runs, but at this level it does not seem to affect significantly the performance of the catalysts. Thus, these catalysts are able to maintain their efficiency at least up to 3 consecutive runs without loss of their structural properties.

4. Conclusion

It has been demonstrated that $MnWO_4$ nanorods are active catalysts for the selective oxidation of cyclohexane at mild conditions, 140-150ºC, with a selectivity to KA oil (cyclohexanol+cyclohexanone) of approximately 85% (determined by use of a heavy solvent injection). Although a low level of carbonaceous material was formed on the catalysts as shown by TGA and FTIR, the catalysts were able to sustain performance in 3 consecutive runs.

The activity of $MnWO_4$ was improved by impregnation of small amounts of Ce, around 1 wt%. Crystallinity and the textural properties of the $MnWO_4$ nanorods were not greatly compromised by low loadings of Ce (1 wt%), and Ce was found to be well-dispersed on the support. XPS analysis of 1%Ce-$MnWO_4$ showed that the oxidation state of Ce was mainly Ce^{3+}, possibly involving some doping of Ce into the $MnWO_4$ surface. The high proportion of Ce^{3+} is assumed to lead to an increased level of oxygen vacancies which provide sites for oxygen activation and mobility. At higher impregnation levels Ce has a detrimental impact on the activity of the $MnWO_4$ nanorods as a result of the formation of a high proportion of Ce^{4+} and blockage of $MnWO_4$ active sites by the presence of large CeO_2 particles, 10-50 nm, heterogeneously distributed over the surface of the $MnWO_4$ nanorods.

The performance of the 1%Ce-$MnWO_4$ catalyst is shown to be stable during 3 consecutive reaction runs. Ce impregnation of $MnWO_4$ nanorods with lower amounts produces promising catalysts for cyclohexane selective oxidation to KA oil with a performance comparable to recently reported mesoporous Ce-Mn oxide solid solutions catalysts [21]. Indeed, it appears that 1%Ce-$MnWO_4$ may be an intrinsically more active material than a Ce-Mn oxide solid solution.

Acknowledgements

This work was supported by King Abdulaziz City of Science and Technology (KACST) under a KOPRC project. We are grateful to Dr. Gwilherm Kerherve for assistance with the XPS analysis and Dr Mahmoud Ardakani for help with TEM.

References

[1] J.A. Labinger, J. E. Bercaw, Understanding and exploiting C-H bond activation, Nature 417 (2002) 417 507-514.

[2] T. Newhouse, P.S. Baran, If C–H bonds could talk: Selective C-H bond oxidation, Angew. Chem. Int. Ed. 50 (2011) 3362-3374.

[3] U. Neuenschwander, N. Turra, C. Aellig, P. Mania, I. Hermans, Understanding selective oxidations, Chimia 64 (2010) 225-230.

[4] J.J. McKetta, W.A. Cunningham, Encyclopedia of Chemical Processing and Design, Marcel Dekker, New York, 1977.

[5] R. Raja, Strategically Designed Single-Site Heterogeneous Catalysts for Clean Technology, Green Chemistry and Sustainable Development, in: K.D.M. Harris, P.P Edwards (Eds.), Turning Points in Solid-State, Materials and Surface Science, Chapter 37, Royal Society of Chemistry, 2007, p. 623-638.

[6] R. Jevtic, P.A. Ramachandran, M.P. Dudukovic, Effect of Oxygen on Cyclohexane Oxidation: A Stirred Tank Study, Ind. Eng. Chem. Res. 48 (2009) 7986-7993.

[7] H. Li, Y. She, T. Wang, Advances and perspectives in catalysts for liquid-phase oxidation of cyclohexane, Front. Chem. Sci. Eng. 6 (2012) 356-368.

[8] P. Khirsariya, R. Mewada, Review of a Cyclohexane Oxidation Reaction Using Heterogenous Catalyst, IJEDR 2 (2014) 3911-3914.

[9] U. Schuchardt, D. Cardoso, R. Sercheli, R. Pereira, R.S. da Cruz, M.C. Guerreiro, D. Mandelli, E.V. Spinacé, E.L. Pires, Cyclohexane oxidation continues to be a challenge, Appl. Catal. A: Gen.211 (2001) 1-17.

[10] S. Van de Vyver, Y.Román-Leshkov, Emerging catalytic processes for the production of adipic acid, Catal. Sci. Technol. 3 (2013) 1465-1479.

[11] X. Duan, W. Liu, L. Yue, W. Fu, M. =N. Ha, J. Li, G. Lua, Selective oxidation of cyclohexane on a novel catalyst Mg–Cu/SBA-15 by molecular oxygen, Dalton Trans. 44 (2015) 17381-17388.

[12] C.R. Riley, N.E. Montgomery, N.N. Megally, J.A. Gunn, L.S. Davis, Oxidation of Cyclohexane by Transition Metal Oxides on Zeolites, The Open Catal. J., 5 (2012) 8-13.

[13] W.-J. Zhou, R. Wischert, K. Xue, Y.-T. Zheng, B. Albela, L. Bonneviot, J.-M. Clacens, F. De Campo, M. Pera-Titus, P. Wu, Highly Selective Liquid-Phase Oxidation of Cyclohexane to KA Oil over Ti-MWW Catalyst: Evidence of Formation of Oxyl Radicals, ACS Catal. 4 (2014) 53-62.

[14] L.-X. Xu, C.-H. He, M.-Q. Zhu, K.-J.Wu, Y.-L. Lai, Silica-Supported Gold Catalyst Modified by Doping with Titania for Cyclohexane Oxidation, Catal. Lett. 118 (2007) 248-253.

[15] L. Zhou, J. Xu, H. Miao, F. Wang, X. Li, Catalytic oxidation of cyclohexane to cyclohexanol and cyclohexanone over Co_3O_4 nanocrystals with molecular oxygen, Appl. Catal. A: Gen. 292 (2005) 223-228.

[16] J. Tonga, L. Boc, Z. Li, Z. Lei, C. Xia, Magnetic $CoFe_2O_4$ nanocrystal: A novel and efficient heterogeneous catalyst for aerobic oxidation of cyclohexane, J. Mol. Catal. A: Chem. 307 (2009) 58-63.

[17] B. Modén, L. Oliviero, J. Dakka, J.G. Santiesteban, E. Iglesia, Structural and Functional Characterization of Redox Mn and Co Sites in AlPO Materials and Their Role in Alkane Oxidation Catalysis, J. Phys. Chem. B 108 (2004) 5552-5563.

[18] M. Wu, W. Zhan, Y. Guo, Y. Wang, Y. Guo, X. Gong, L. Wang, G. Lu, Solvent-free selective oxidation of cyclohexane with molecular oxygen over manganese oxides: Effect of the calcination temperature, Chin. J. Catal. 37 (2016) 184-192.

[19] X. Li, T. Lunkenbein, J. Kröhnert, V. Pfeifer, F. Girgsdies, F. Rosowski, R. Schlögl, A. Trunschke, Hydrothermal synthesis of bi-functional nanostructured manganese tungstate catalysts for selective oxidation, Faraday Discuss. 188 (2016) 99-113.

[20] X. Li, T. Lunkenbein, V. Pfeifer, M. Jastak, P.K. Nielsen, F. Girgsdies, A. Knop-Gericke, F. Rosowski, R. Schlögl, A. Trunschke, Selective Alkane

Oxidation by Manganese Oxide: Site Isolation of MnOx Chains at the Surface of MnWO4 Nanorods, Angew. Chem. Int. Ed. 55 (2016) 4092-4096.

[21] P. Zhang, H. Lu, Y. Zhou, L. Zhang, Z. Wu, S. Yang, H. Shi, Q. Zhu, Y. Chen, S. Dai, Mesoporous MnCeOx solid solutions forlow temperature and selective oxidationof hydrocarbons, Nat. Commun. 6:8446 (2015) 1-10.

[22] A. Selvamani, M. Selvaraj, M. Gurulakshmi, R. Ramya, K. Shanthi, Selective Oxidation of Cyclohexane Using $Ce_{1-x}Mn_xO_2$ Nanocatalysts, J. Nanosci. Nanotechnol. 14 (2014) 2864-2870.

[23] P. Venkataswamy, K.N. Rao, D. Jampaiah, B.M. Reddy, Nanostructured manganese doped ceria solid solutions for CO oxidation at lower temperatures, Appl. Catal. B: Environ. 162 (2015) 122-132.

[24] B. Agula, Q.-F. Deng, M.-L. Jia,Y. Liu, B. Zhaorigetu, Z.-Y. Yuan, Catalytic oxidation of CO and toluene over nanostructured mesoporous $NiO/Ce_{0.8}Zr_{0.2}O_2$ catalysts, Kinet. Mech. Catal. 103 (2011) 101-112.

[25] H. Li, G. Q. Tana, X. Zhang, W. Li, W. Shen, Morphological impact of manganese–cerium oxides on ethanol oxidation, Catal. Sci. Technol. 1 (2011) 1677-1682.

[26] M.J. Beier, T.W. Hansen, J.-D. Grunwaldt, Selective liquid-phase oxidation of alcohols catalyzed by a silver-based catalyst promoted by the presence of ceria, J. Catal. 266 (2009) 320-330.

[27] S. Zhao, R.J. Gorte, A comparison of ceria and Sm-doped ceria for hydrocarbon oxidation reactions, Appl. Catal. A: Gen. 277 (2004) 129-136.

[28] W. Zhan, G. Lu, Y. Guo, Y. Guo, Y. Wang, Y. Wang, Z. Zhang, X. Liu, Synthesis of cerium-doped MCM-48 molecular sieves and its catalytic performance for selective oxidation of cyclohexane, J. Rare Earths, 26 (2008) 515-522.

[29] D. Delimaris, T. Loannides, VOC oxidation over MnO_x-CeO_2 catalysts prepared by a combustion method, Appl. Catal. B: Environ. 84 (2008) 303-312.

[30] E. Ramirez-Cabrera, A. Atkinson, D. Chadwick, Reactivity of Gd and Nb doped ceria to methane, App. Catal. B: Environ. 36 (2002) 193-206.

[31] S.-H. Yu, B. Liu, M.-S. Mo, J.-H. Huang, X.-M. Liu, Y.-T. Quian, General synthesis of single-crystal tungstate nanorods/nanowires: A facile, low-temperature solution approach, Adv. Funct. Mater. 13 (2003) 639-647.

[32] G.B. Shul'pin, Metal-catalyzed hydrocarbon oxygenations in solutions: the dramatic role of additives: a review, J. Mol. Catal. A: Chem. 189 (2002) 39-66.

[33] T.-D. Nguyen, D. Mrabet, T.-T.-D. Vu, C.-T. Dinh, T.-O. Do, Biomolecule-assisted route for shape-controlled synthesis of single-crystalline $MnWO_4$ nanoparticles and spontaneous assembly of polypeptide-stabilized mesocrystal microspheres, Cryst. Eng. Comm. 13 (2011) 1450-1460.

[34] H.W. Nesbitt, D. Banerjee, Interpretation of XPS Mn(2p) spectra of Mn oxyhydroxides and constraints on the mechanism of MnO_2 precipitation, American Mineralogist 83 (1998) 305-315.

[35] A.J. Nelson, J.G. Reynolds, J.W. Roos, Core level satellites and outer core level splitting in Mn model compounds, J. Vac. Sci. Technol. A, 18(2000)1072-1076

[36] M.C. Biesinger,B.P. Payne, A.P Grosvenor, L.W.M. Lau, A.R.Gerson, R.St.C. Smart, Resolving surface chemical states in XPS analysis of first row transition metal oxides and hydroxides, App. Surf. Sci. 257(2011)2717-2730

[37] R.J. Iwanowski, M.H. Heinonen, E.Janik, X-ray photoelectron spectra of zinc blende MnTe, Chem. Phys. Lett. 387(2004)110-115

[38] X. Wu, H. Yu, D. Weng, S. Liu, J. Fan, Synergistic effect between MnO and CeO_2 in the physical mixture: Electronic interaction and NO oxidation activity, J. Rare Earths, 31 (2013) 1141-1147.

[39] M.M. Hejazi, E. Taghaddos, A. Safari, Reduced leakage current and enhanced ferroelectric properties in Mn-doped $Bi_{0.5}Na_{0.5}TiO_3$-based thin films, J. Mater. Sci. 48 (2013) 3511-3516.

[40] F.A.C. Garcia, D.R. Araújo, J.C.M. Silva, J.L. de Macedo, G.F. Ghesti, S.C.L. Dias, G.N.R. Filho, Effect of Cerium Loading on Structure and Morphology of Modified Ce-USY Zeolites, J. Braz. Chem. Soc. 22 (2011) 1894-1902.

[41] C.R. Moreira, M.M. Pereira, X. Alcobé, N. Homs, J. Llorca, J.L.G. Fierro, P.R. de la Piscina, Nature and location of cerium in Ce-loaded Y zeolites as revealed

by HRTEM and spectroscopic techniques, Microp. Mesop. Mater. 100 (2007) 276-286.

[42] E. Beche, P. Charvin, D. Perarnau, S. Abanades, G. Flamant, Ce 3d XPS investigation of cerium oxides and mixed cerium oxide ($Ce_xTi_yO_z$), Surf. Interface Anal. 40 (2008) 40 264-267.

[43] D. Chadwick, J. McAleese, K. Senkiw, B.C.H. Steele, On the application of XPS to ceria films grown by MOCVD using a fluorinated precursor, Appl. Surf. Sci. 99 (1996) 417-420.

[44] L. Chen, J. Li, W. Ablikim, J. Wang, H. Chang, L. Ma, J. Xu, M. Ge, H. Arandiyan, CeO_2-WO_3 Mixed Oxides for the Selective Catalytic Reduction of NO_x by NH_3 Over a Wide Temperature Range, Catal. Lett. 142 (2011) 1859-1864.

[45] T. Skala, V. Matolin, Growth of cerium tungstate epitaxial layers: influence of temperature, Surf. Interface Anal. 48 (2016) 111-114.

[46] R. Jevtic, P.A. Ramachandran, M.P. Dudukovic, Effect of Oxygen on Cyclohexane Oxidation: A Stirred Tank Study, Ind. Eng. Chem. Res. 48 (2009) 7986-7993.

[47] B. Stuart, Infrared Spectroscopy: Fundamentals and Applications, John Wiley & Sons, Ltd, 2004.

[48] E. Ramirez-Cabrera, A. Atkinson, D. Chadwick, Influence of point defects on the resistance of ceria to carbon deposition in hydrocarbon catalysis, Solid State Ionics 136 (2000) 825-831.

Table 1. BET surface area and crystallinity for the pure $MnWO_4$ and doped with Ce.

Sample	S_{BET} (m^2/g)	Crystallinity (%)
$MnWO_4$	14	100
1%Ce-$MnWO_4$	13	76
3%Ce-$MnWO_4$	14	69
5%Ce-$MnWO_4$	12	65

Table 2. Reaction rates for the $MnWO_4$ and 1%Ce-$MnWO_4$ catalysts at 140 and 150ºC.

Reaction rate (mmol/g/h)	140ºC	150ºC
$MnWO_4$	8.9	18.7
1%Ce-$MnWO_4$	8.3	37.7

Table 3. Cyclohexyl-hydroperoxide selectivities (%) vs. reaction time for the $MnWO_4$ at 140 and 150ºC.

time (h)	140ºC	150ºC
1	24	30
2	11	19
3	10	9
4	13	4
6	5	0
8	-	5

Table 4. Cyclohexyl-hydroperoxide selectivities (%) vs. reaction time for the 1%Ce-$MnWO_4$ at 140 and 150ºC.

time (h)	140ºC	150ºC
1	13	12
1.5	10	11
2	10	14
4	14	5
6	10	1
8	1	0

Table 5. Conversion to KA oil, yields and selectivities obtained for the $MnWO_4$ catalyst during 3 consecutive reaction runs at 150ºC.

Run	Conversion (%)	Yield (%)			Selectivity (%)		
		CyHOH	CyHO	CyHOOH	CyHOH	CyHO	CyHOOH
1	6.15	3.00	2.92	0.23	49	47	4
2	5.78	3.08	2.68	0.03	53	46	0.4
3	5.87	3.02	2.66	0.20	51	45	3

CyHOH = cyclohexanol; CyO = cyclohexanone; CyHOOH = cyclohexyl-hydroperoxide.

Table 6. Conversion to KA oil, yields and selectivities obtained for the 1%Ce-$MnWO_4$ catalyst during 3 consecutive reaction runs at 150ºC.

Run	Conversion (%)	Yield (%)			Selectivity (%)		
		CyHOH	CyHO	CyHOOH	CyHOH	CyHO	CyHOOH
1	7.08	3.44	3.28	0.37	49	46	5
2	7.18	3.61	3.57	0	50	50	0
3	7.42	3.69	3.73	0	50	50	0

CyHOH = cyclohexanol; CyO = cyclohexanone; CyHOOH = cyclohexyl-hydroperoxide.

Figure captions

Fig. 1: XRD diffraction patterns for pure $MnWO_4$, $MnWO_4$ impregnated with Ce, bulk CeO_2, $MnWO_4$ spent sample and 1%Ce-$MnWO_4$ spent sample.

Fig. 2: TEM micrographs for the **(a)** $MnWO_4$ including SAED **(b)** 1%Ce-$MnWO_4$, **(c)** 5%Ce-$MnWO_4$, **(d)** 5%Ce-$MnWO_4$, detail of a Ce oxide particles on the surface.

Fig. 3: (a) Mn 2p, **(b)** W 4f, **(c)** O 1s XPS spectra for $MnWO_4$.

Fig. 4: (a) Mn 2p, **(b)** W 4f, **(c)** O 1s, **(d)** Ce 3d XPS spectra for the 1% and 5%Ce-$MnWO_4$.

Fig 5: Conversion to KA oil as a function of the reaction time for $MnWO_4$ and 1%Ce-$MnWO_4$ catalysts at **(a)** 140°C, **(b)** 150°C. Standard deviations in conversion (a) $MnWO_4$ at 6h = 0.6, 1%Ce-$MnWO_4$ at 4h = 0.1, (b) $MnWO_4$ at 2h = 0.4, 4h = 0.3, 8h = 0.2, 1%Ce-$MnWO_4$ at 2h = 0.1, 6h = 0.1.

Fig 6: Cyclohexanol (■) and cyclohexanone (Δ) selectivities as a function of reaction time for $MnWO_4$ (closed symbols) and 1%Ce-$MnWO_4$ (open symbols) catalysts at **(a)** 140°C, **(b)** 150°C. Standard deviations in selectivities (a) $MnWO_4$ at 6h = 2.8, 1%Ce-$MnWO_4$ at 4h = 0.4, (b) $MnWO_4$ at 2h = 0.3, 4h = 2.8, 4h = 1.1, 1%Ce-$MnWO_4$ at 2h = 0.1, 6h = 1.8.

Fig. 7: Conversion to KA oil (black), cyclohexanol yield (dark grey), cyclohexanone yield (medium grey) and cyclohexyl-hydroperoxide yield (light grey) for $MnWO_4$ and $MnWO_4$ impregnated with Ce at **(a)** 140°C, **(b)** 150°C after 4h reaction time.

Fig 8: (a) Conversion to KA oil for $MnWO_4$, $MnWO_4$ + CeO_2 mechanical mixtures, and 1%Ce-$MnWO_4$ at 150°C after 2h reaction time. **(b)** Relative increase of the conversion for the $MnWO_4$ + CeO_2 mechanical mixtures compared to $MnWO_4$ as a function of the amount of CeO_2. Standard deviations in conversion (a) 1%Ce = 0.2, 3%Ce = 0.5, 5%Ce = 0.1.

Fig. 1

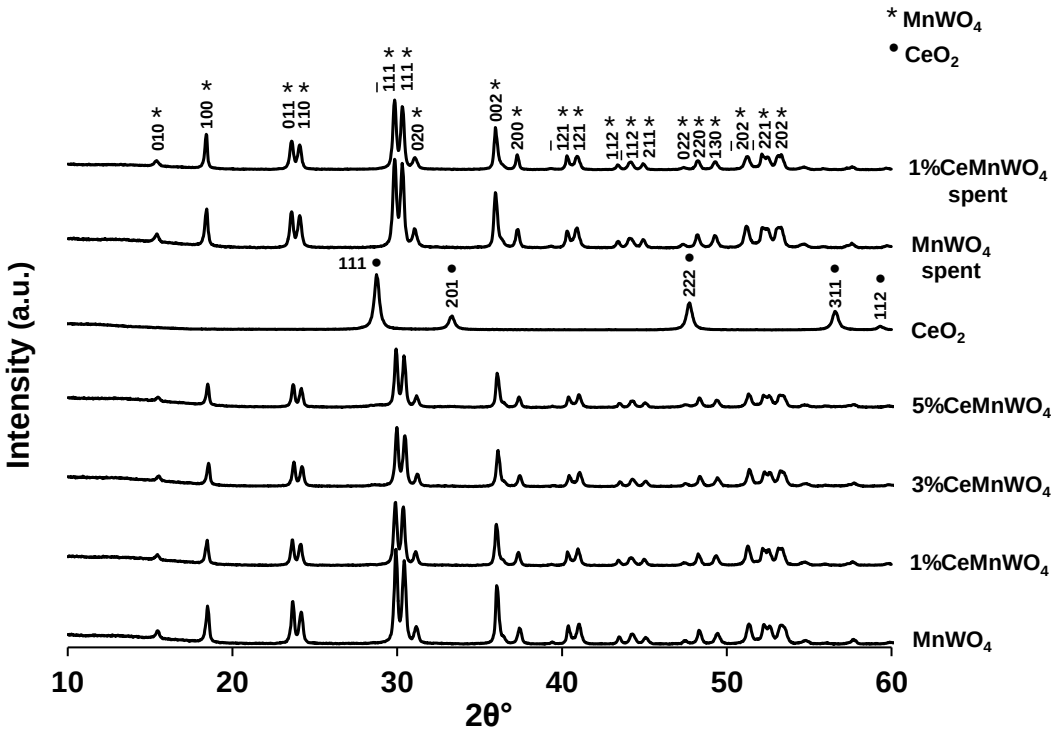
* MnWO4
• CeO2
010 *
100 *
011 *
110 *
-111 *
111 *
020 *
002 *
200 *
-121 *
121 *
-112 *
112 *
211 *
022 *
220 *
130 *
-202 *
221 *
202 *
1%CeMnWO4 spent
MnWO4 spent
111 •
201 •
222 •
311 •
112 •
CeO2
5%CeMnWO4
3%CeMnWO4
1%CeMnWO4
MnWO4
Intensity (a.u.)
10
20
30
40
50
60
2θ°

Fig. 2

(a)

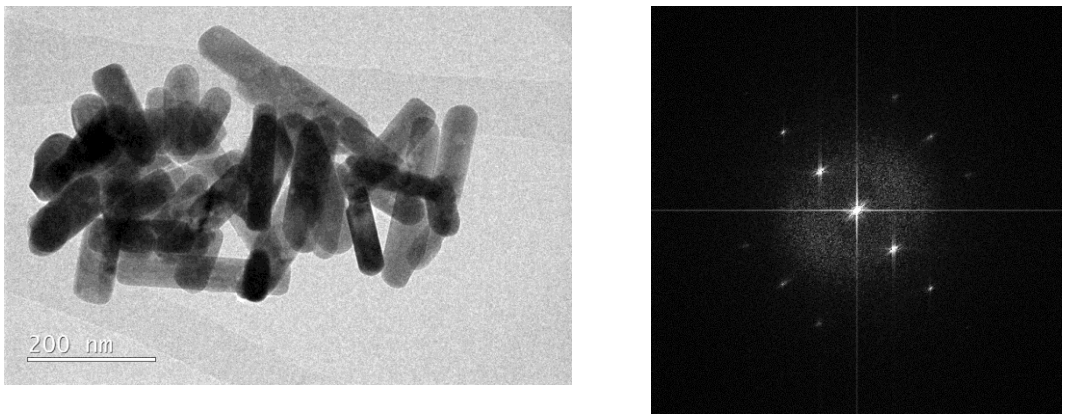

(b)

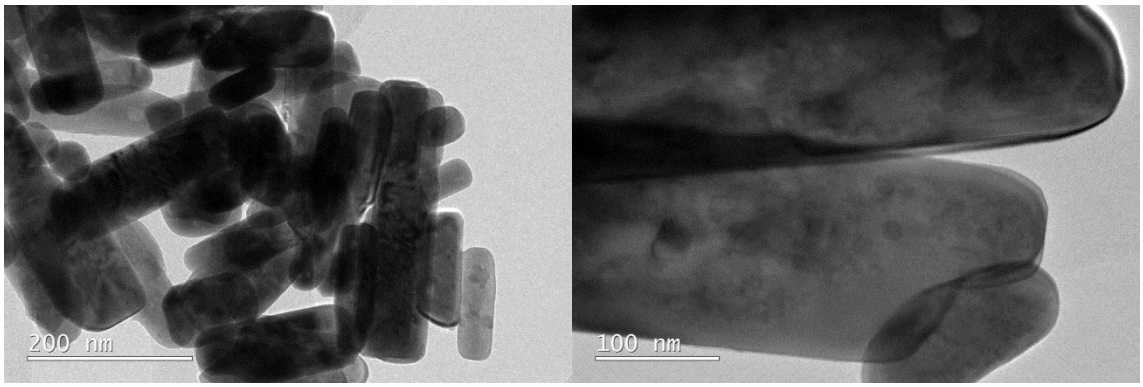

(c)

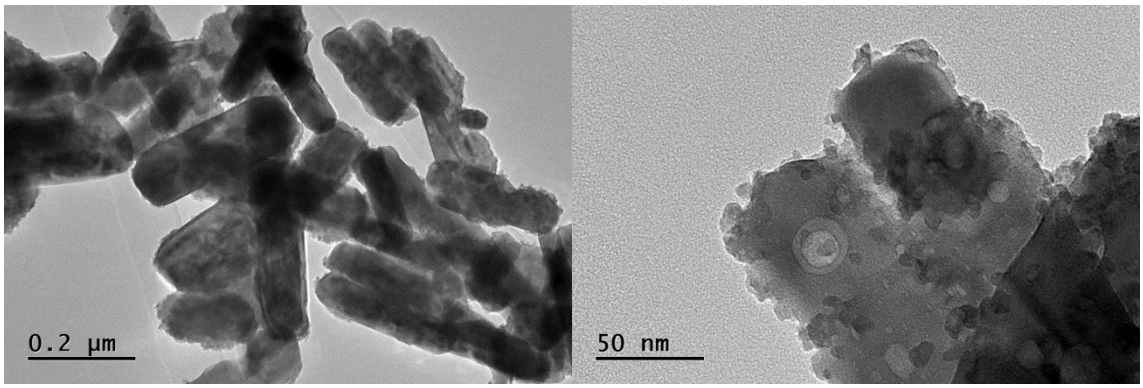

(d)

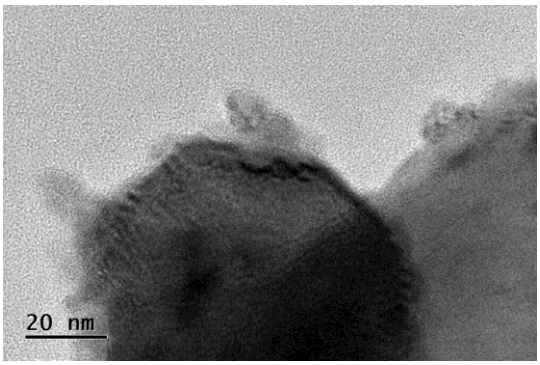

Fig. 3

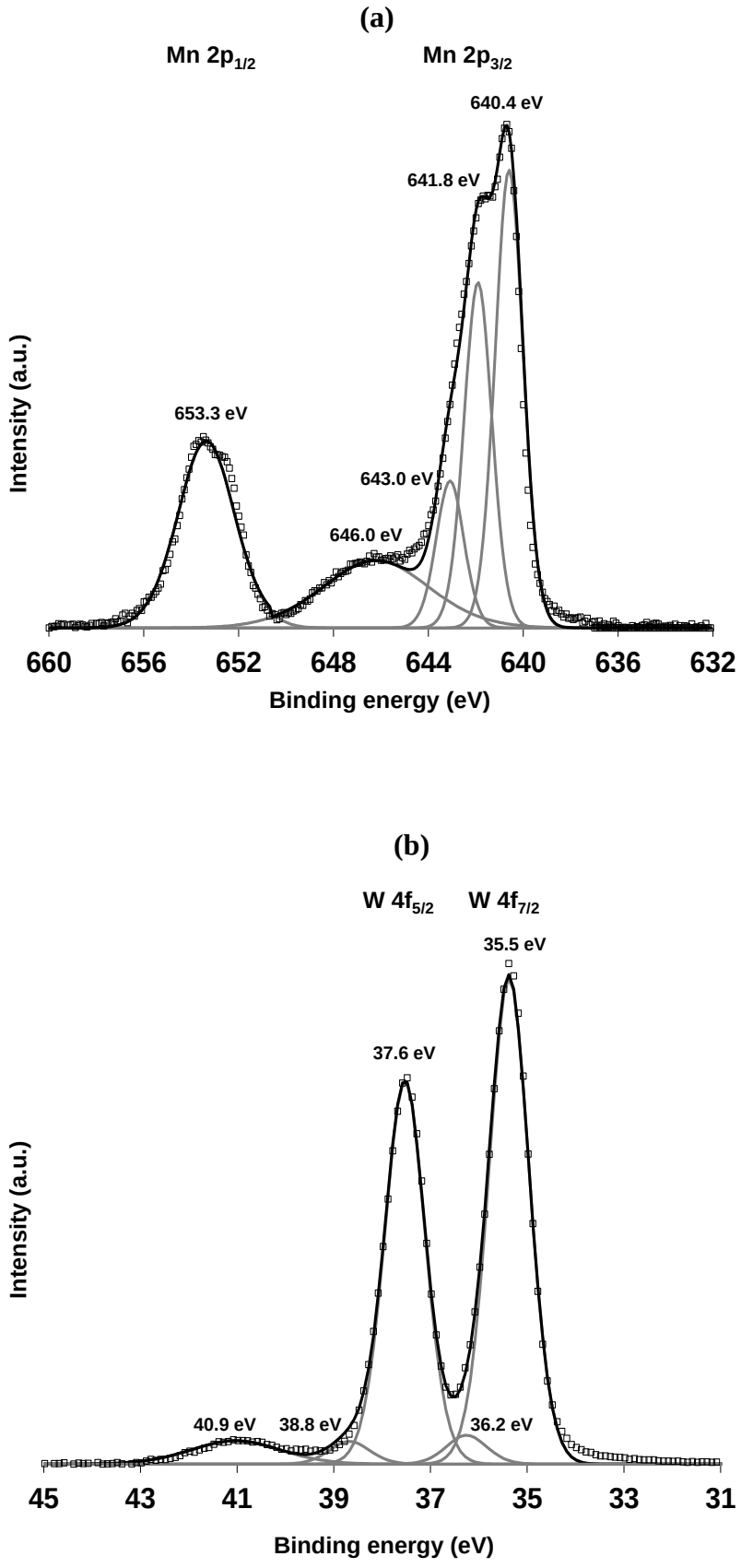
(a)
Mn 2p1/2
Mn 2p3/2
640.4 eV
641.8 eV
653.3 eV
643.0 eV
646.0 eV
Intensity (a.u.)
660
656
652
648
644
640
636
632
Binding energy (eV)
(b)
W 4f5/2
W 4f7/2
35.5 eV
37.6 eV
40.9 eV
38.8 eV
36.2 eV
Intensity (a.u.)
45
43
41
39
37
35
33
31
Binding energy (eV)

(c)

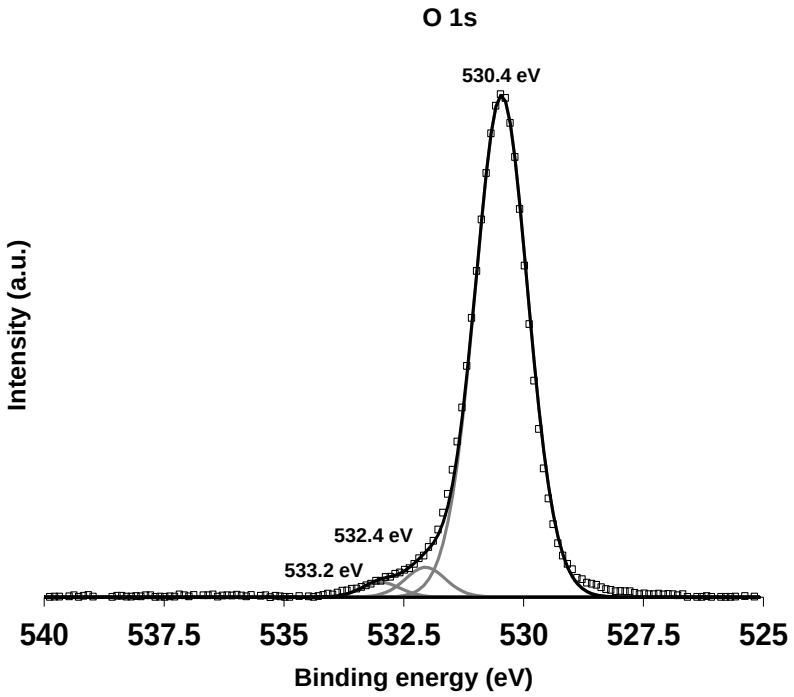
O 1s
530.4 eV
532.4 eV
533.2 eV
Intensity (a.u.)
540
537.5
535
532.5
530
527.5
525
Binding energy (eV)

Fig. 4

(a)

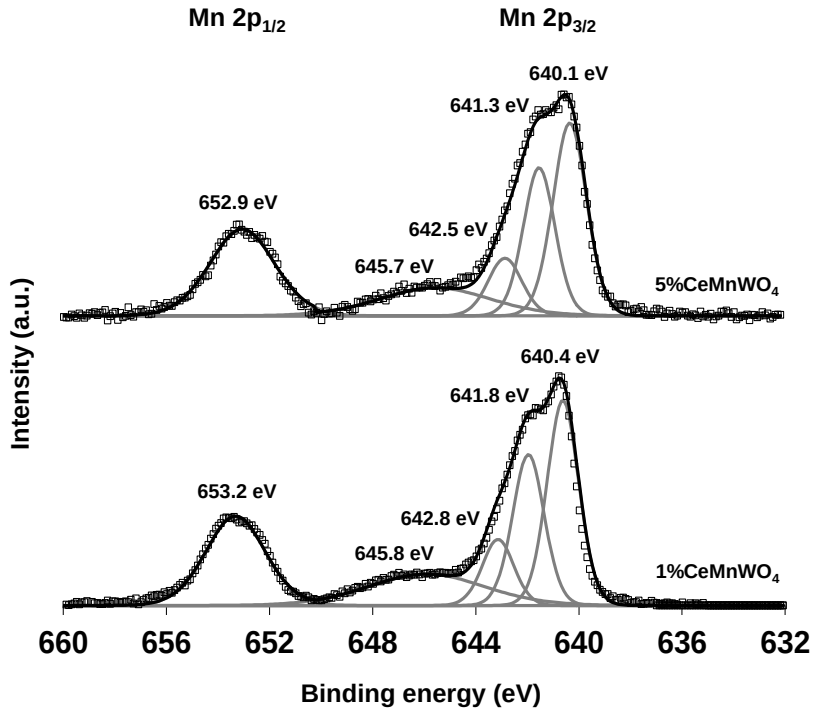
Mn 2p1/2
Mn 2p3/2
640.1 eV
641.3 eV
652.9 eV
642.5 eV
645.7 eV
5%CeMnWO4
640.4 eV
641.8 eV
653.2 eV
642.8 eV
645.8 eV
1%CeMnWO4
Intensity (a.u.)
660
656
652
648
644
640
636
632
Binding energy (eV)

(b)

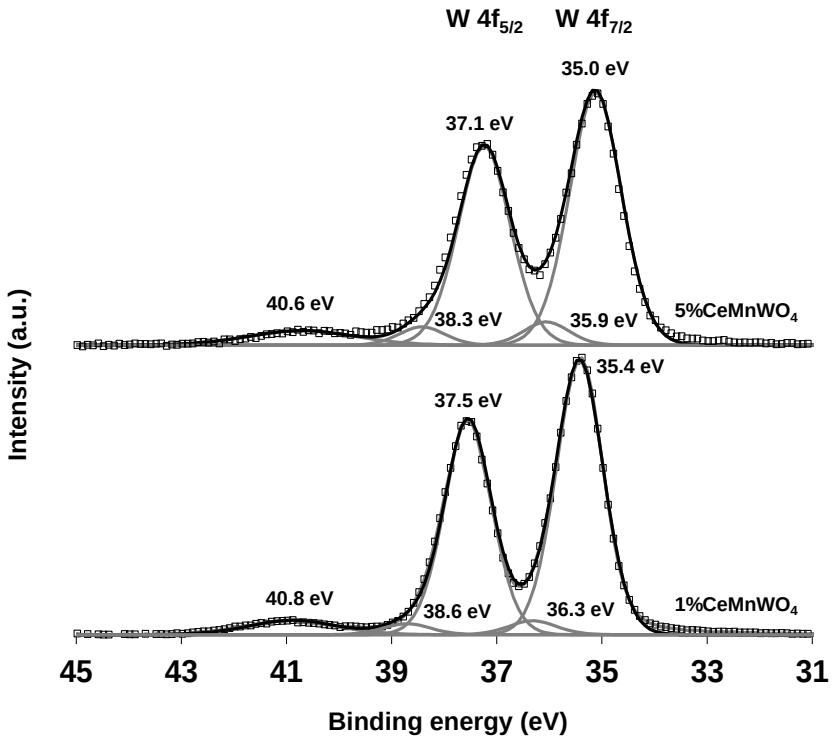
W 4f5/2
W 4f7/2
35.0 eV
37.1 eV
40.6 eV
38.3 eV
35.9 eV
5%CeMnWO4
35.4 eV
37.5 eV
40.8 eV
38.6 eV
36.3 eV
1%CeMnWO4
Intensity (a.u.)
45
43
41
39
37
35
33
31
Binding energy (eV)

(c)

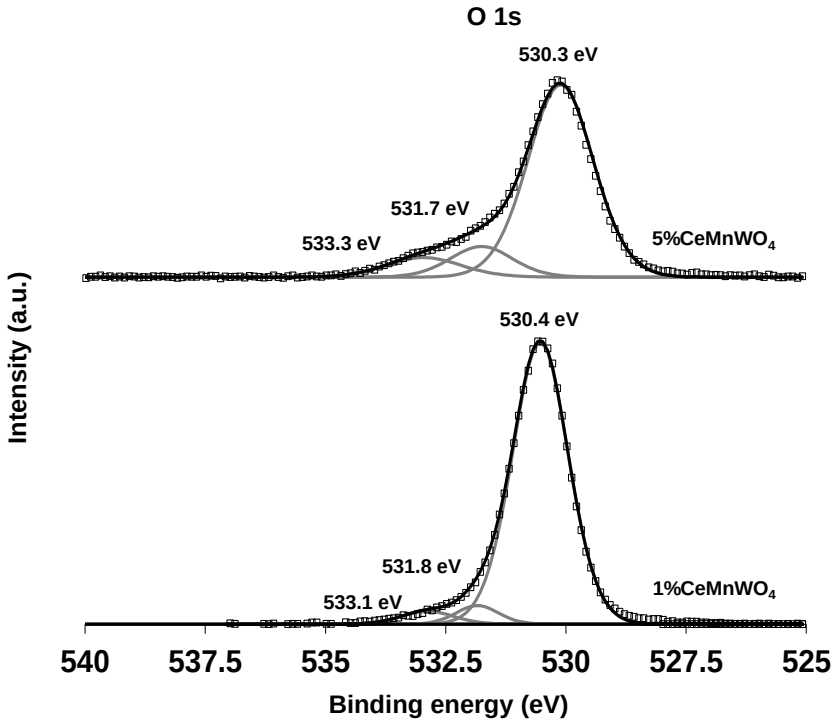
O 1s
530.3 eV
531.7 eV
533.3 eV
5%CeMnWO4
530.4 eV
531.8 eV
533.1 eV
1%CeMnWO4
Intensity (a.u.)
540
537.5
535
532.5
530
527.5
525
Binding energy (eV)

(d)

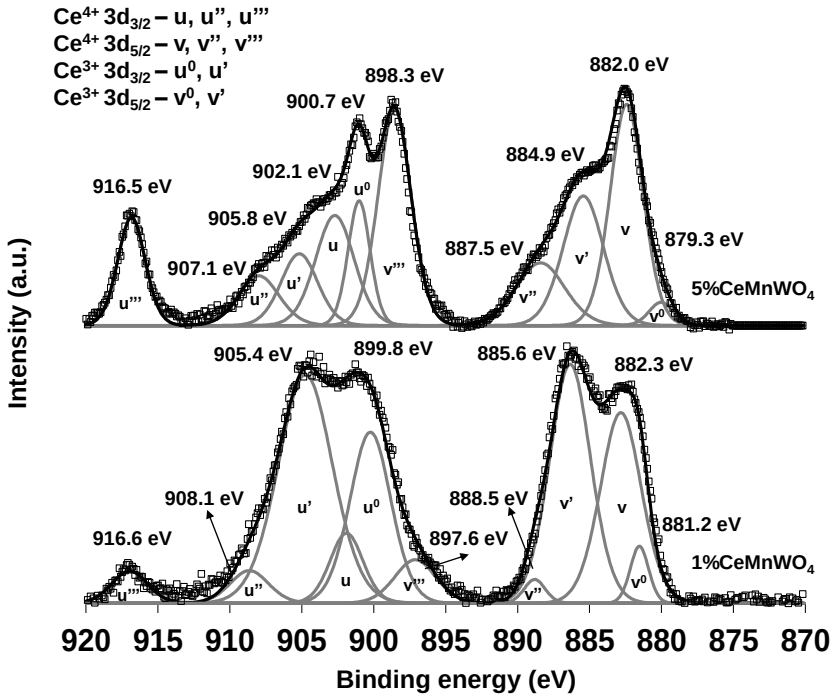
Ce4+ 3d3/2 – u, u'', u'''
Ce4+ 3d5/2 – v, v'', v'''
Ce3+ 3d3/2 – u0, u'
Ce3+ 3d5/2 – v0, v'
916.5 eV
907.1 eV
905.8 eV
902.1 eV
900.7 eV
898.3 eV
887.5 eV
884.9 eV
882.0 eV
879.3 eV
5%CeMnWO4
916.6 eV
908.1 eV
905.4 eV
899.8 eV
897.6 eV
888.5 eV
885.6 eV
882.3 eV
881.2 eV
1%CeMnWO4
Intensity (a.u.)
920
915
910
905
900
895
890
885
880
875
870
Binding energy (eV)

Fig. 5

(a)

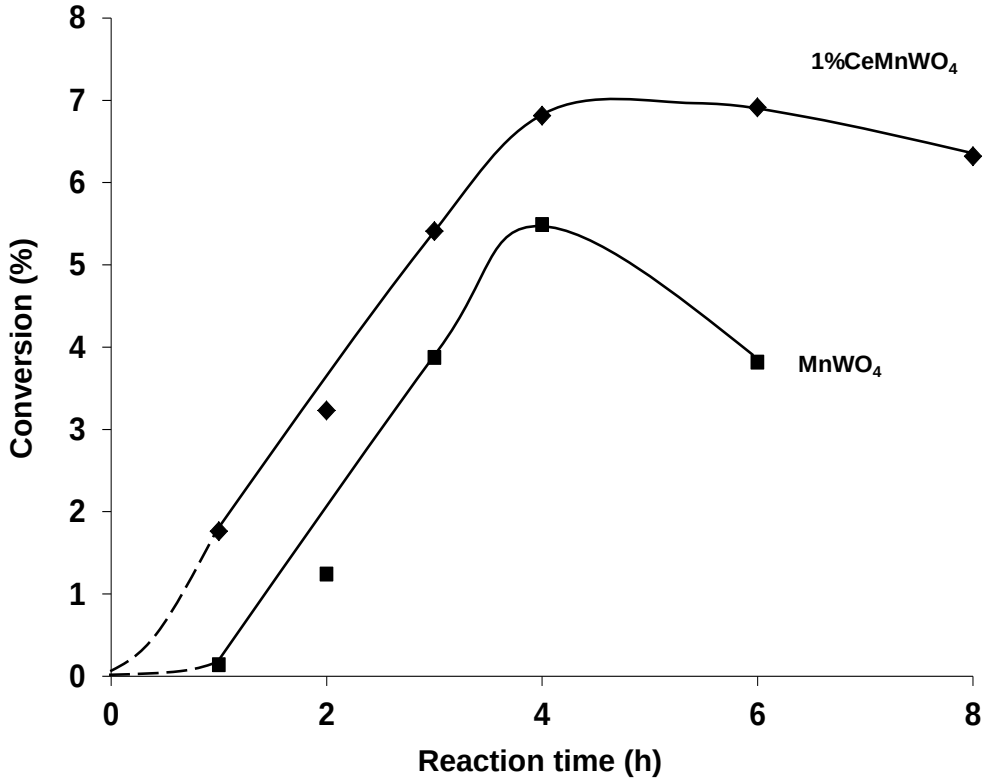
Conversion (%)
Reaction time (h)
1%CeMnWO4
MnWO4
0
1
2
3
4
5
6
7
8
0
2
4
6
8

(b)

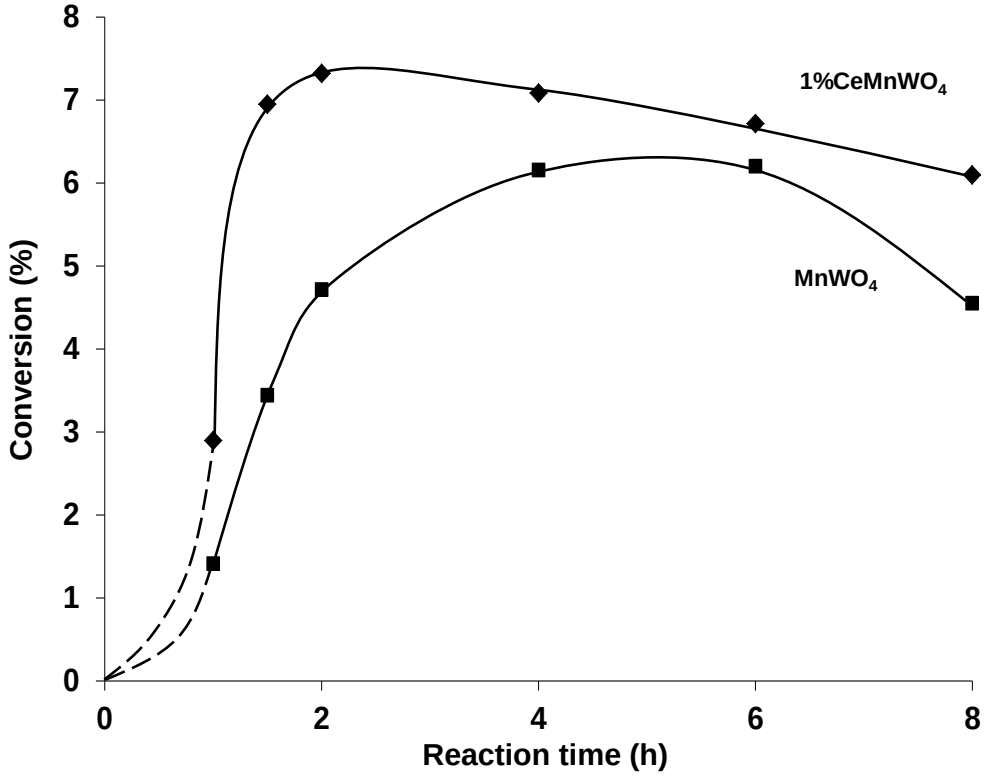
Conversion (%)
Reaction time (h)
1%CeMnWO4
MnWO4
0
1
2
3
4
5
6
7
8
0
2
4
6
8

Fig. 6

(a)

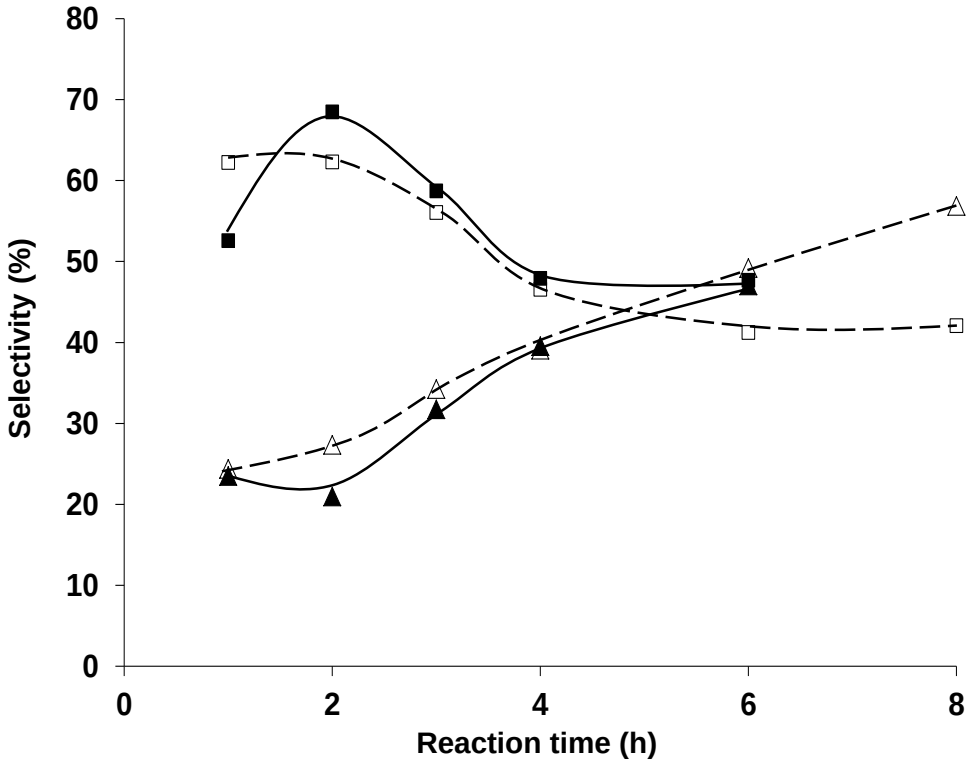
Selectivity (%)
Reaction time (h)
0
10
20
30
40
50
60
70
80
0
2
4
6
8

(b)

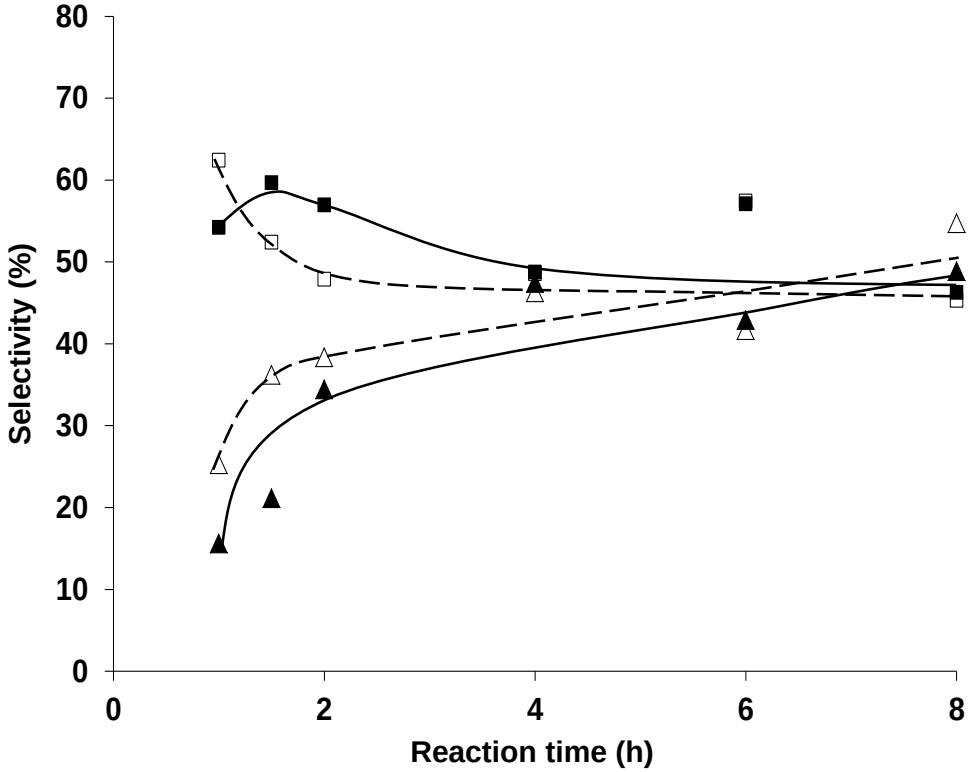
Selectivity (%)
Reaction time (h)
0
10
20
30
40
50
60
70
80
0
2
4
6
8

Fig. 7

(a)

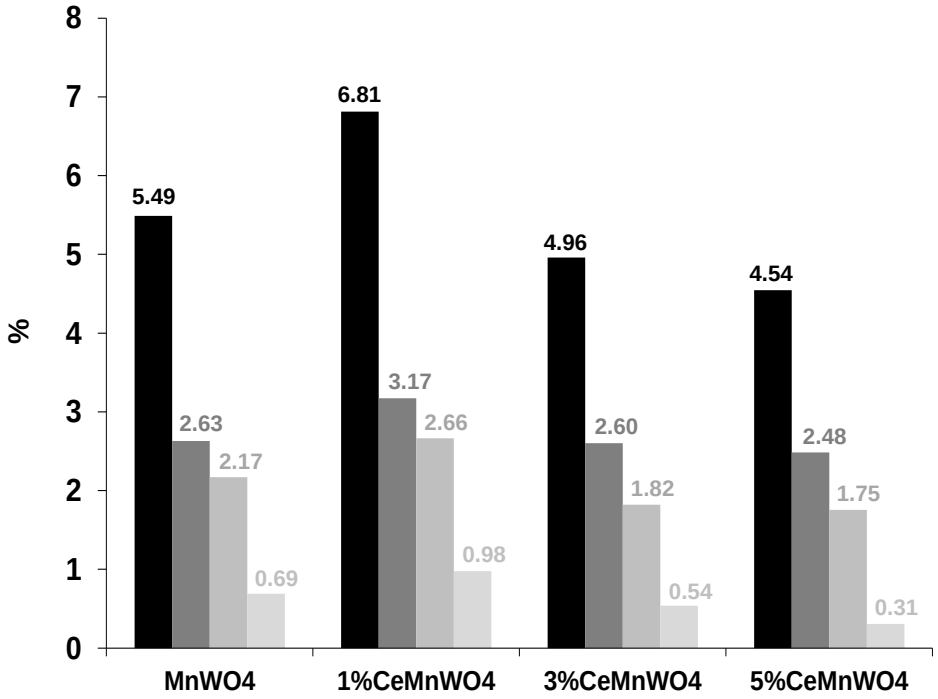
%
0
1
2
3
4
5
6
7
8
5.49
2.63
2.17
0.69
6.81
3.17
2.66
0.98
4.96
2.60
1.82
0.54
4.54
2.48
1.75
0.31
MnWO4
1%CeMnWO4
3%CeMnWO4
5%CeMnWO4

(b)

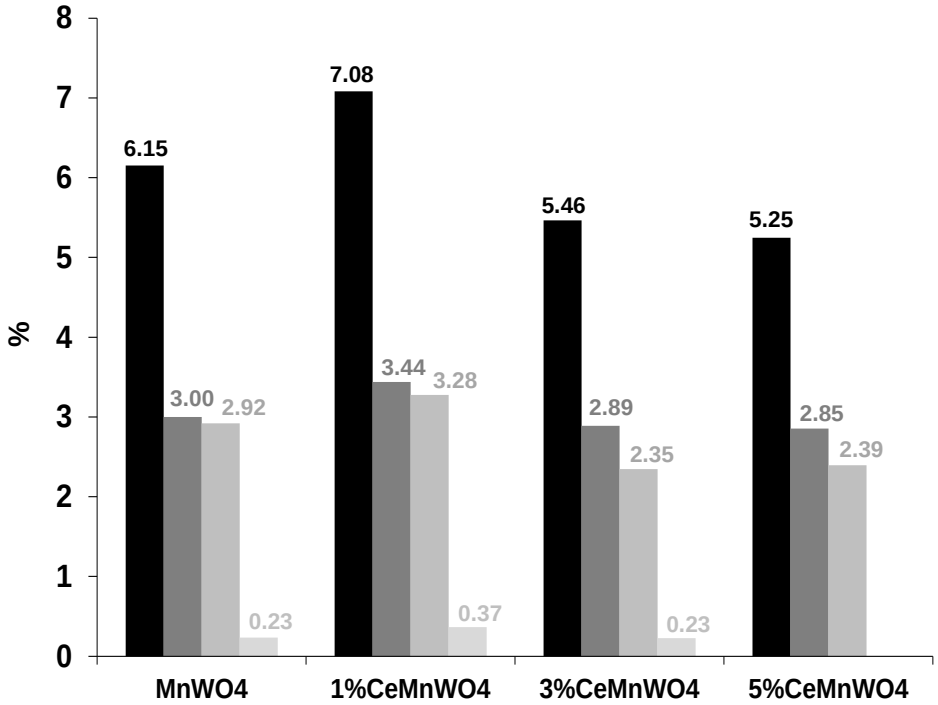
%
0
1
2
3
4
5
6
7
8
6.15
3.00
2.92
0.23
7.08
3.44
3.28
0.37
5.46
2.89
2.35
0.23
5.25
2.85
2.39
MnWO4
1%CeMnWO4
3%CeMnWO4
5%CeMnWO4

Fig. 8

(a)

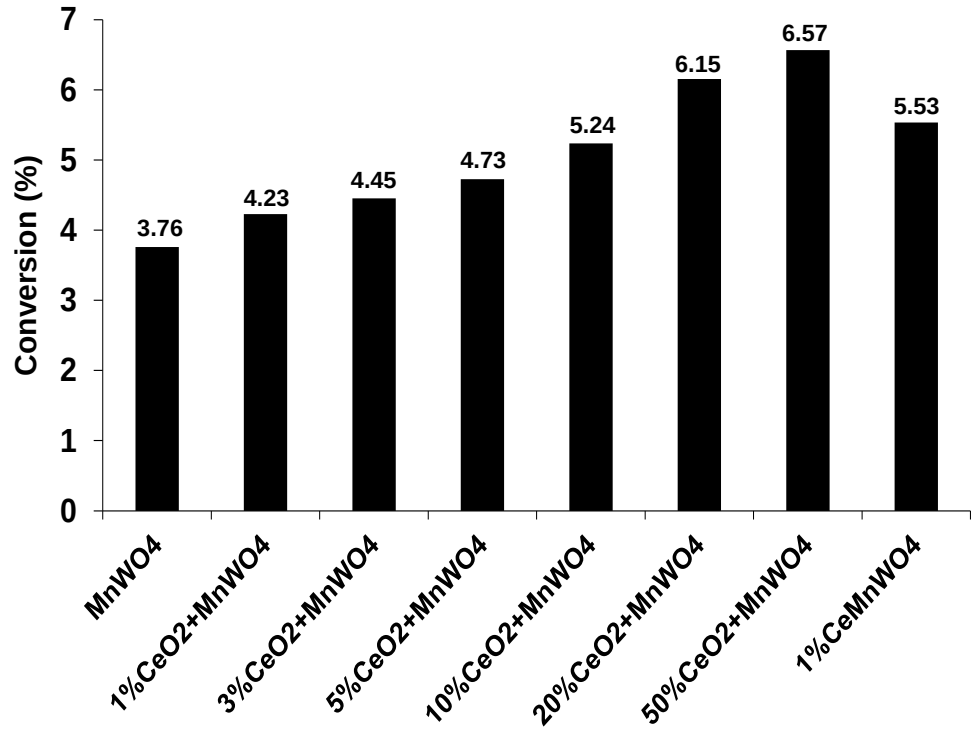
Conversion (%)
0
1
2
3
4
5
6
7
3.76
4.23
4.45
4.73
5.24
6.15
6.57
5.53
MnWO4
1%CeO2+MnWO4
3%CeO2+MnWO4
5%CeO2+MnWO4
10%CeO2+MnWO4
20%CeO2+MnWO4
50%CeO2+MnWO4
1%CeMnWO4

(b)

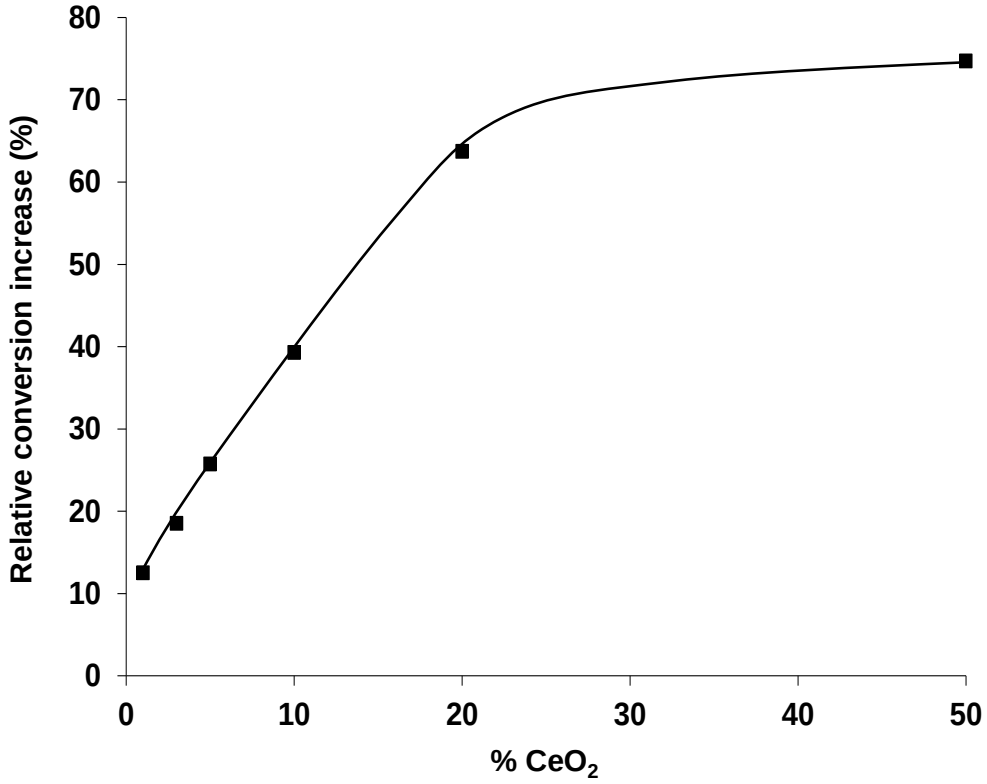
Relative conversion increase (%)
0
10
20
30
40
50
60
70
80
0
10
20
30
40
50
% CeO2